Chapter 3
Interfacing Silicon Nanophotonic Integrated Circuits and Single-Mode Optical Fibers with Diffraction Gratings

Günther Roelkens and Dries Van Thourhout

Abstract Exploiting the high refractive index contrast achievable on the silicon-on-insulator (SOI) material platform enables a drastic scaling down of the footprint of integrated optical functions. While this allows for large-scale integration of optical functions, it severely complicates the interfacing with a single-mode optical fiber, due to the huge mismatch in mode size between the optical fiber and nanophotonic silicon waveguide. In this chapter we elaborate on the use of diffraction gratings to achieve an efficient, compact, alignment-tolerant, polarization-independent, and broadband optical coupling. Besides using these components as an interface with an optical fiber, its use to interface with opto-electronic components will be discussed. Finally, an optical probe will be presented, based on a diffraction grating integrated on the facet of a single-mode fiber. Such an optical probe allows testing of individual components in a silicon-on-insulator nanophotonic integrated circuit.

3.1 Nanophotonic SOI Waveguide Circuits

Silicon-on-insulator (SOI) is emerging as the most important platform for large-scale photonic integrated circuits. This is due to the high refractive index contrast between the silicon waveguide core and SiO_2 or air cladding. This huge refractive index contrast allows a drastic reduction in the size of individual optical functions, bringing large-scale integrated optical circuits closer to reality. Moreover, these photonic integrated circuits can be fabricated using standard CMOS technology on 200-mm or 300-mm wafers [1]. This allows for low-cost mass manufacturing and leverages from the billion dollar investments done in the development of stable

G. Roelkens (✉)
Photonics Research Group, Department of Information Technology, Ghent University/IMEC, B-9000 Ghent, Belgium
e-mail: Gunther.Roelkens@intec.ugent.be

D. Van Thourhout (✉)
Photonics Research Group, Department of Information Technology, Ghent University/IMEC, B-9000 Ghent, Belgium
e-mail: Dries.Vanthourhout@intec.ugent.be

D.J. Lockwood, L. Pavesi (Eds.): *Silicon Photonics II.*
Topics in Applied Physics **119**, 71–94 (2011)
DOI 10.1007/978-3-642-10506-7_3

and high-yield processes for CMOS manufacturing. While the degree of scaling is a clear merit of the use of high refractive index contrast waveguide systems like silicon-on-insulator, it severely complicates the interfacing with an optical fiber. This is clear from the huge mismatch between the modal area of a single-mode optical fiber (≈100 μm^2) and that of a nanophotonic monomode waveguide (≈0.1 μm^2). This is perhaps one of the most important issues that high-index contrast waveguide circuits face for practical applications.

3.2 Solutions to the Fiber-Chip Coupling Problem

Various solutions to the fiber-chip coupling problem have been proposed in the literature. The most common solution implies the use of a spot size converter to transform the size of the mode of the nanophotonic waveguide to that of the optical fiber. In principal, a three-dimensional adiabatic taper structure can be used for this purpose, both laterally and vertically transforming the size of the silicon waveguide [2]. The technology required to do this is, however, not CMOS compatible, thereby compromising its use in practical applications. A second approach to change the spot size on the photonic integrated circuit is to use a lateral inverted taper structure. In these structures, the width of the silicon nanophotonic waveguide is tapered down to sub 100-nm dimensions (which can be achieved using state-of-the-art deep UV lithography used in CMOS fabrication), thereby expanding the size of the optical mode. By realizing a low refractive index waveguide on top of this inverted taper structure, very efficient coupling can be obtained between the nanophotonic waveguide and the low refractive index waveguide [3]. However, to interface with a single-mode fiber, this requires a low refractive index waveguide with cross-sectional dimensions comparable to that of the single-mode fiber core. This approach therefore suffers from two important drawbacks: the integration of such a large core optical waveguide requires a huge topography (to CMOS standards) on the photonic integrated circuit, compromising further processing. Moreover, to adiabatically transform the mode from a nanophotonic silicon waveguide to such a large core waveguide would require taper structures of thousands of micrometers in length, thereby canceling out the advantages of using a high-index contrast waveguide system for increasing the density of optical functions on the SOI chip. This is why in current implementations, the use of inverted adiabatic taper structures is limited to interfacing with a lensed optical fiber, since this reduces the topography on the integrated circuit to about 3 μm (which is still large, but manageable) and reduces the taper length to hundreds of microns, a more typical length scale in high-index contrast waveguide circuits. This approach allows for a high efficiency (an insertion loss lower than 1 dB has been shown) and large optical bandwidth (typically several hundreds of nanometers) coupling between a lensed fiber and a nanophotonic integrated circuit [3]. It however requires the use of specialty optical fiber and the associated small alignment tolerances. Besides the requirement of a specialty optical fiber, maybe the most important issue with this approach is the requirement of a cleaved and polished facet to interface with the photonic

integrated circuit. While this is the standard approach for current photonic integrated circuits (like planar lightwave circuits, edge-emitting laser diodes, etc.), the advent of large-scale photonic integrated circuits requires a fiber coupling approach that does not require singulated chips for optical interfacing, e.g., for optical testing on a wafer scale, comparable to the wafer scale electrical testing in electronic integrated circuits.

Therefore the use of a new type of optical interface between a standard single-mode fiber and nanophotonic waveguide circuit using diffractive grating structures was proposed [4]. In these coupling structures, the lateral adaptation of the mode size is achieved by a conventional in-plane taper structure. The interfacing with the optical fiber, however, is done by redirecting the light exiting the photonic integrated circuit out of the plane of the photonic integrated circuit, using a diffraction grating (vice versa for optical coupling to the photonic integrated circuit). In this way the optical fiber interfaces with the silicon photonic integrated circuit from the top, no longer requiring a singulated chip for coupling. This approach even enables packaging on the wafer level, by integrating fiber alignment structures on the wafer level. These two aspects, namely the possibility of wafer scale testing and wafer level packaging of photonic integrated circuits, could enable a dramatic reduction in the cost of the photonic integrated circuit, since these are two of the most cost-intensive operations in the whole fabrication cycle of the device. In the subsequent sections we will outline the operation principle, the design and the experimental realization of high efficiency, wide band and polarization independent grating coupler structures. We will show that, besides their use as fiber-chip couplers, they can also be used to interface a silicon photonic integrated circuit with a (flip-chipped) opto-electronic component. In Fig. 3.1, the three approaches discussed above for fiber-chip coupling are schematically depicted.

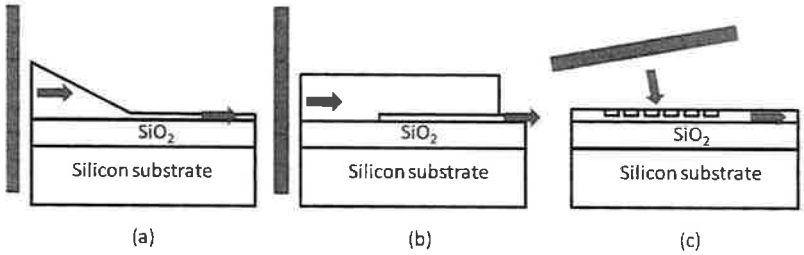

Fig. 3.1 Comparison of two spot-size converter approaches (3D adiabatic tapering in (**a**), lateral inverted tapers in (**b**)) to interface with an optical fiber and (**c**) the diffractive grating based coupling

3.3 Fundamentals of Fiber-Chip Diffraction Grating Couplers

In its most simple form, a diffractive grating coupler consists of a one-dimensional periodic structure defined on or in the silicon waveguide layer (later on we will show that also two-dimensional periodic structures can be used), as shown in Fig. 3.2a.

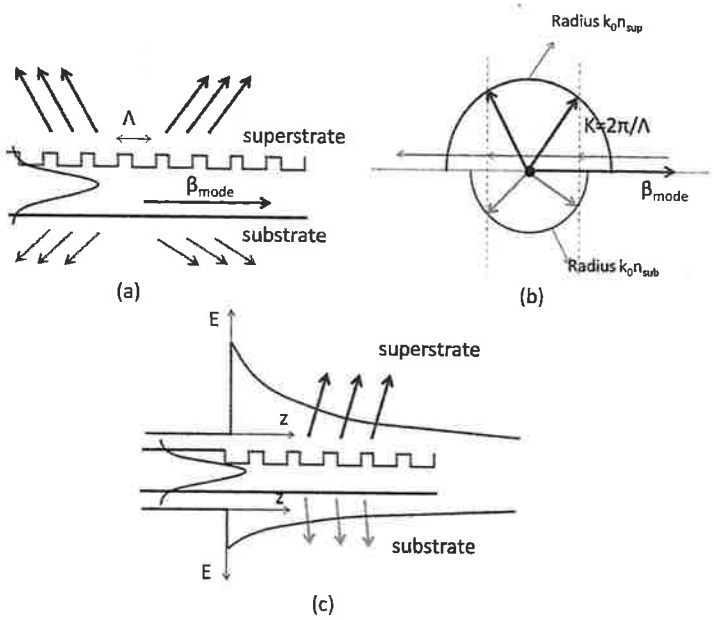

Fig. 3.2 Fundamental operation principle of a one-dimensional diffraction grating structure: (**a**) device layout, (**b**) geometric representation of the projected Bragg condition, and (**c**) the exponential decay of the diffracted field profile

The periodicity implies that light is diffracted from these structures in preferential directions. This can be understood by looking at the one-dimensional grating structure as a collection of scatter centers (located at the interface between the slits and teeth of the grating), which have a fixed phase relation due to the periodicity of the structure. This fixed phase relation results in a strongly angle-dependent interference. For infinitely extending periodic structures, this interference behavior can be mathematically described by the projected Bragg condition

$$k_{z,m} = \beta_{\mathbf{mode}} + mK \tag{3.1}$$

with m an integer. In this formula $k_{z,m}$ is the z-component of the wave vector of the diffracted wave of the mth order (which arises due to the fact that all scatter centers interfere constructively in a particular direction). $\beta_{\mathbf{mode}}$ is the effective wave vector of the optical mode in the silicon grating. In low-index contrast grating structures this is approximately the propagation constant of the guided mode in the uncorrugated waveguide section. In a high refractive index contrast structure this perturbation analysis is no longer valid and the effective propagation constant is an average of the propagation constant of the guided mode in the unetched and etched

waveguide region. $\boldsymbol{K}$ is the reciprocal lattice vector of the periodic structure. Its length is given by $K = \frac{2\pi}{\Lambda}$ with Λ the period of the diffraction grating.

The projected Bragg condition directly determines the angle of diffraction, since $k_z = \frac{2\pi n \sin\theta_0}{\lambda}$, with n the refractive index of the medium in which the diffracted wave is propagating. Therefore the diffraction angle θ_0 is determined by

$$\sin\theta_0 = \frac{n_{\text{eff}}(\lambda)}{n} + m\frac{\lambda}{n\Lambda} \tag{3.2}$$

since $\beta_{\text{mode}} = \frac{2\pi n_{\text{eff}}(\lambda)}{\lambda}$. The right hand side of this equation has to be in between -1 and 1 for diffraction to occur. By properly choosing the grating period Λ (for a given λ,$n_{\text{eff}}(\lambda)$ and n) one can realize a grating in which diffraction occurs into only one diffraction order, i.e., only the diffraction order $m = -1$ is present. This is the preferred situation for the fiber-chip grating couplers, which we will describe in this chapter, since it allows efficient collection of the light diffracted from the grating, by positioning the single-mode optical fiber on top of the grating structure at an angle corresponding to the diffraction angle of this single diffraction order. A geometrical representation of this projected Bragg condition is shown in Fig. 3.2b.

The choice of the diffraction angle depends on the particular application. Typically an angle between 8 and 15° off vertical is chosen. The reason why an off-surface normal coupling angle is chosen becomes clear from the Bragg diffraction. To obtain the condition of perfectly vertical coupling to the chip, the length of the reciprocal lattice vector has to obey

$$K = \beta_{\text{mode}} \tag{3.3}$$

since $m = -1$. Although this condition indeed produces only a single order of diffraction into the superstrate, a second-order reflection also occurs, back into the waveguide, since

$$k_{z,-2} = \beta_{\text{mode}} - 2K = -\beta_{\text{mode}} \tag{3.4}$$

The second-order reflection toward the photonic integrated circuit is unwanted and reduces the coupling efficiency to the optical fiber. Therefore a slightly off-normal operating grating coupler is typically used (a so-called detuned grating), since in this case no second-order Bragg reflection occurs. In Sect. 3.7, we will elaborate on how this performance reduction for vertical incidence can be avoided, for the integration of surface emitting opto-electronic components on the silicon photonics platform.

The Bragg formalism described above is only valid for infinitely extending structures. In the design of the fiber-chip grating couplers, one has to take into account the finite (or at least the semi-infinite) nature of the diffraction grating. When the optical mode in the silicon input waveguide is exciting the diffraction grating, optical power is coupled out of the waveguide layer during the propagation due to diffraction

(besides some scattering at the interface between the access waveguide and the grating, due to a slight mismatch between the waveguide mode and the grating mode). This results in an exponentially decaying diffracted field profile (different from the plane wave considered in infinitely extending structures). This exponentially decaying field profile, as shown in Fig. 3.2c has two consequences: first of all, it can be considered as a superposition of plane waves that propagate at an angle θ centered around θ_0, with an amplitude distribution $A(\theta)$ determined by the Fourier transform of this exponentially decaying field profile. The extent of the angular distribution of these plane wave components is therefore inversely proportional to the decay length of the diffracted field. This implies that a grating with a strong refractive index contrast (resulting in a short decay length) generates a whole range of plane waves. Since the angle θ_0 only varies slowly with wavelength (typically 1°/10 nm), a large optical bandwidth coupling can be realized in high-index contrast grating structures, which will be discussed in more detail in Sect. 3.5. A second consequence of the exponentially decaying diffracted field profile is the fact that there is a mismatch with the Gaussian fiber mode in a single-mode optical fiber. This limits the achievable fiber coupling efficiency for a uniform grating structure. These aspects will be discussed in the following sections.

So far, the influence of the polarization of the incident light has not yet been considered. Due to the high refractive index contrast obtained in silicon-on-insulator waveguide circuits, these waveguides show a strong modal birefringence. This implies that the diffraction angle for transverse electric and transverse magnetic polarized light is substantially different, making these one-dimensional diffraction gratings very polarization dependent. In Sect. 3.6 we will describe, however, how we can utilize this strong polarization dependence to realize a polarization diversity approach based on two-dimensional diffraction gratings, effectively rendering the photonic integrated circuit polarization independent. For the one-dimensional grating structures described in the subsequent sections, transverse electric (TE) polarized light is always assumed, with the dominant electrical field component oriented along the grating lines.

3.4 High-Efficiency Fiber-Chip Grating Couplers

Simply calculating the overlap between the exponentially decaying field profile and the Gaussian mode profile of a single-mode fiber (with a $1/e^2$ intensity mode field diameter of 10.4 μm) shows that there is an optimal decay length in the diffracted field profile of $L = 7.6\,\mu$m, for which the overlap integral is maximal [4]. This results in a minimal insertion loss of about 1 dB for uniform grating couplers. While this theoretical minimal loss can be improved by the use of non-uniform diffraction gratings, where the coupling strength of the grating structure varies along the grating, this is not considered in this chapter, since it requires the definition of features which cannot be defined and/or well controlled by state-of-the-art deep UV lithography.

While there is a 1 dB theoretical limit in the achievable fiber coupling efficiency for one-dimensional uniform diffraction grating structures, there is another, more prominent, loss mechanism in these devices. So far, we have only considered the light that is diffracted toward the optical fiber. However, since the refractive index of the buried oxide layer, separating the silicon waveguide layer from the silicon substrate, has a comparable index to that of the superstrate (either air, SiO_2 or index matching glue), diffraction also occurs toward the silicon substrate, as is clear from Fig. 3.2. This limits the directionality of the grating structure (being defined as the ratio of the optical power diffracted toward the optical fiber to the total diffracted optical power). In a basic diffraction grating structure, where the one-dimensional grating is defined by etching in the silicon waveguide layer, typically a 50% directionality is obtained, implying that only a maximum coupling efficiency of −4 dB (−3 dB from the limited directionality and −1 dB from the mode profile mismatch) can be obtained. Therefore, tackling this problem is, in a first phase, more critical than trying to match the mode profiles.

To improve the directionality, we envisaged two types of solutions, schematically outlined in Fig. 3.3. In one type of solution, the downward diffracted light from the grating was redirected upward by integrating a mirror below the grating structure. Both a metallic mirror and distributed Bragg reflector mirror were considered. While in this case a very high directionality is obtained, care has to be taken to optimize the distance between this bottom mirror and the grating. This is due to the fact that the

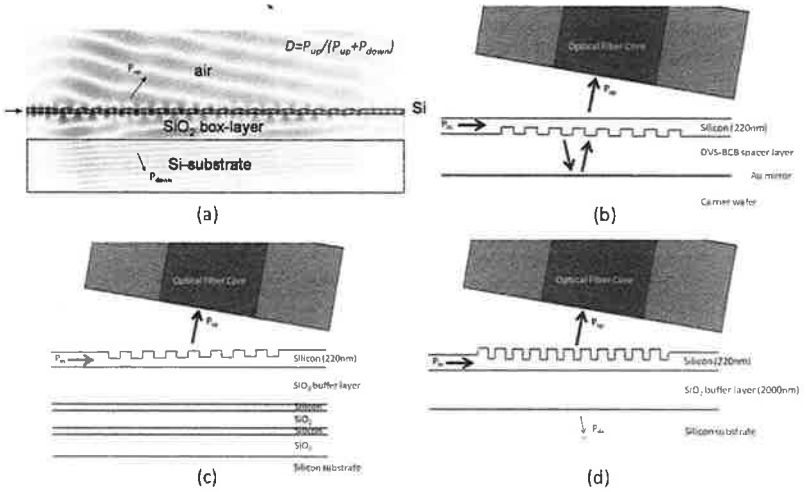

Fig. 3.3 Schematic outline of the different strategies pursued to realize high efficiency fiber-to-chip grating couplers: (**a**) the standard – moderate efficiency – grating coupler structure with the grating lines directly etched in the silicon waveguide layer, (**b**) the metallic and (**c**) DBR type bottom mirror approach, and (**d**) the silicon overlay approach

optical field reflected on the bottom mirror will interfere with the directly upward diffracted wave. This interference modifies the coupling strength of the grating (i.e., when there is destructive interference between both diffracted waves, little light will be coupled out of the grating and hence the coupling length will be very long). Since one still needs to obtain a grating coupling length matched to the dimensions of the single-mode optical fiber, care has to be taken in optimizing these structures.

Device optimization of the bottom mirror grating structures was performed using finite difference time domain (FDTD) and eigenmode expansion methods. To limit the required computational resources, simulations are limited to two-dimensional simulations. This is a good approximation for one-dimensional fiber-chip grating couplers, since the waveguides are in practice 12 μm wide (i.e., 24 material wavelengths) to interface with a single-mode fiber. While this shows that the diffracted field profile coming from a two-dimensional simulation corresponds well to the full three-dimensional simulation, still a correction factor of 0.97 (on a linear scale) in the fiber-chip coupling efficiency needs to be taken into account, due to the slight mismatch in lateral field profile between the silicon waveguide mode (approximately cosinusoidal) and the Gaussian fiber mode. In Fig. 3.4a and b, the electric field component (for TE polarized light) of the diffraction in each type of optimized grating structure is plotted.

Both a metallic bottom mirror-based fiber-chip grating coupler [5] and a DBR bottom mirror-based fiber-chip grating coupler [6] were experimentally realized. For the metallic mirror approach, a 50-nm-thick layer of gold was used. The bottom mirror diffraction grating was realized used a wafer bonding approach. In

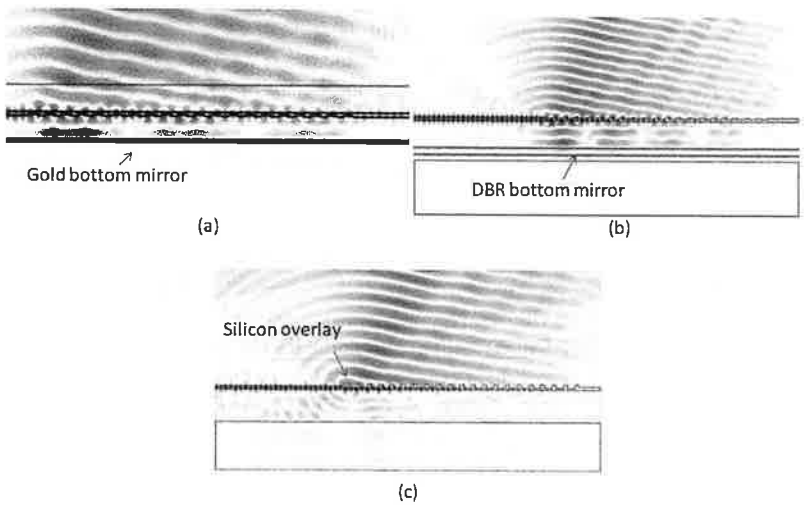

Fig. 3.4 Simulation results for the optimized grating structures for the different strategies pursued to realize high efficiency fiber-to-chip grating couplers: (**a**) gold bottom mirror approach, (**b**) DBR type bottom mirror approach, and (**c**) the silicon overlay approach

this approach a uniform one-dimensional grating structure was defined on an SOI waveguide wafer using the standard lithography and etching processes. Afterwards a polymer (DVS-BCB) spacer layer was applied, after which the gold mirror is defined on top of the grating coupler structure. Finally, the waveguide layer is transferred to a silicon carrier wafer substrate using a DVS-BCB bonding technique. After removal of the silicon substrate, using the buried oxide layer as an etch stop layer, the grating structure is accessible from the top by an optical fiber. While this approach allows the integration of a bottom mirror below a crystalline silicon waveguide layer, the layer transfer process required to achieve this is not standard CMOS technology. Therefore, a DBR bottom mirror approach was considered, building up the DBR/waveguide layer stack by means of chemical vapor deposition of silicon dioxide and amorphous silicon (a-Si) on a 200-mm wafer scale. In this case a two pair SiO_2/a-Si DBR mirror was used. The experimentally obtained fiber coupling efficiency was in both cases about −1.5 dB, approaching the theoretical limit of a uniform one-dimensional grating structure. The 1 dB optical bandwidth of these coupling structures is approximately 35 nm. In Fig. 3.5, microscope images and SEM images of the fabricated grating structures are shown, together with the experimentally obtained fiber coupling efficiency spectrum. As is clear from these results, a dramatic improvement in coupling efficiency can be obtained compared to a standard, directly etched grating coupler. The parameters of these fabricated devices are listed in Table 3.1 in the appendix to this chapter.

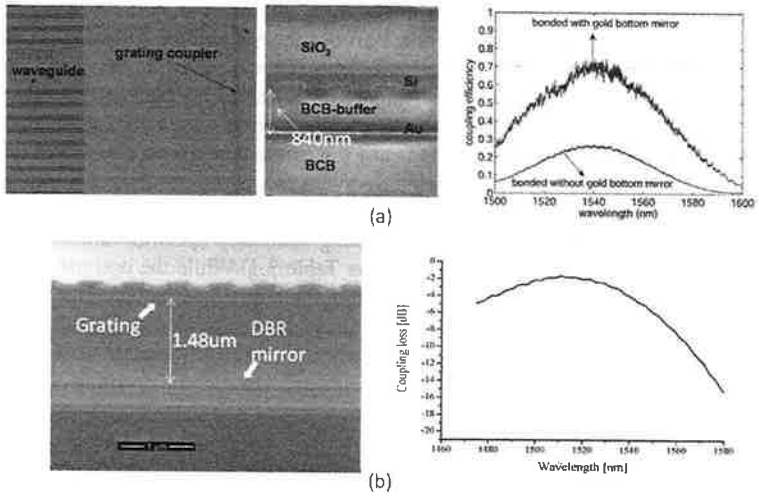

Fig. 3.5 Microscope image and SEM cross-section image of the fabricated high-efficiency grating coupler structures based on a bottom mirror approach, together with the experimentally obtained fiber coupling efficiency spectrum: (**a**) the metallic bottom mirror approach [5] and (**b**) the DBR bottom mirror approach [6]. The DBR consists of two 112-nm-thick a-Si layers with a 267-nm layer of SiO_2 in between

While the integration of a bottom mirror allows for high-efficiency couplers, the drawback is that either a wafer bonding approach is needed or that the silicon waveguide layer is an amorphous silicon layer (e.g., problematic for the integration of high speed modulators). Therefore, another approach was investigated allowing for high-efficiency coupling to a crystalline silicon waveguide layer, in which only CMOS technology is used for the fabrication. The mechanism here to realize high-efficiency coupling is to intrinsically modify the grating directionality by modifying its design. The proposed fabrication procedure consists of the definition of a silicon overlay mesa in the area where the grating will be defined, prior to etching the grating lines [7]. While the optimal design originated from a pure optimization process, the operation principle of the device can be understood as follows. Modifying the design of the grating by having this silicon overlay allows the grating to be designed in such a way that the different scattering centers (which have a fixed phase relation) interfere constructively in the direction of the optical fiber while destructive interference is obtained toward the substrate. Hence, an enhanced directionality can be obtained. Besides the high directionality, the coupling length also needs to be optimized to match with the dimensions of the Gaussian fiber mode (unless a lens system is used to transform the waist of the Gaussian beam as in [9]). Both requirements can be achieved by optimizing the silicon overlay thickness and grating etch depth. Simulations show that in this way efficiencies close to the −1 dB theoretical coupling limit can be obtained.

High-efficiency diffraction gratings based on the silicon overlay approach were fabricated using CMOS technology. The silicon overlay was defined using silicon epitaxial growth in an opened SiO_2 mask layer. Experimentally, a coupling efficiency of −2.6 dB was obtained with a 1 dB optical bandwidth of 50 nm [8]. This is below the expected −1 dB coupling efficiency due to the fact that the fabricated device dimensions deviated from the designed ones. Taking into account the dimensions of the actual fabricated structure, an excellent agreement is obtained between the two-dimensional FDTD simulations and the experimentally obtained fiber coupling spectrum, strengthening our belief that with an optimized fabrication process a −1 dB coupling efficiency is obtainable. SEM images of the fabricated structures and the experimentally obtained fiber coupling efficiency spectrum are shown in Fig. 3.6. The device parameters are listed in Table 3.1. While the optimal grating layer thickness is on the order of 350–400 nm, the optimal waveguide layer thickness still is lower (about 220 nm) in order to obtain a vertically single mode strip waveguide.

3.5 Multi-band Fiber-Chip Grating Couplers

The fiber-chip coupling structures that were outlined in the previous section all show a 1-dB (3 dB) optical bandwidth in the order of 40–50 nm (80–100 nm). While this is sufficient for applications where only a single wavelength band needs to interface with the photonic integrated circuit, a set of applications require a more broadband

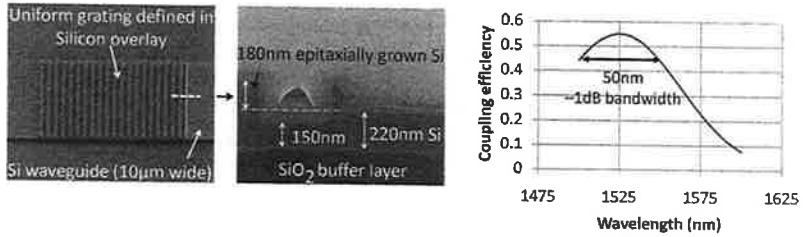

Fig. 3.6 (**a**) SEM images and (**b**) measured fiber-chip coupling efficiency spectrum of a silicon overlay-based grating coupler [8]

optical interface since optical signals in different wavelength bands need to be processed by the photonic integrated circuit. This is, for example, the case in integrated transceivers for optical access networks, where both a 1,310 nm optical signal (i.e., for upstream at the subscriber side) and a 1,490/1,550 nm optical signal (for the downstream analog and digital signal) needs to be coupled to the photonic integrated circuit.

This type of application can also benefit from the use of a diffraction grating to interface with an optical fiber. In this case both access waveguides to the one-dimensional grating structure are being used, as shown in Fig. 3.7a [10]. This allows the diffraction grating to be designed such that the Bragg condition is satisfied for both wavelength bands, by coupling one wavelength band in the forward direction and the second wavelength band in the opposite direction. This approach therefore allows not only to efficiently couple both wavelength bands to the photonic integrated circuit, it also realizes wavelength duplexing, which is required, for example, in the integrated transceiver application. For optimal performance, all device parameters need to be optimized: fiber tilt angle, grating period, grating etch depth, duty cycle, and number of grating periods. This can be achieved using dedicated optimization algorithms such as particle swarm or genetic optimization algorithms, written around the two-dimensional FDTD and eigenmode expansion simulations. The same methods as in the case of a single wavelength band grating coupler discussed in the previous section can be used to increase the fiber coupling efficiency. For example, using a silicon overlay approach to increase the directionality of the grating structures allows realizing a coupling efficiency of about −2.5 dB, for both a 1,310- and 1,490-nm wavelength as shown in Fig. 3.7b. The respective 3 dB optical bandwidth is 55 and 60 nm.

An important issue for these grating duplexer structures, especially when they are used in an upstream/downstream configuration, is the parasitic coupling of the (out-coupled) upstream wavelength channel into the downstream waveguide, resulting in cross-talk (see Fig. 3.7a). While in a grating structure that is optimized for optimal coupling efficiency for both wavelength bands a substantial fraction of the light

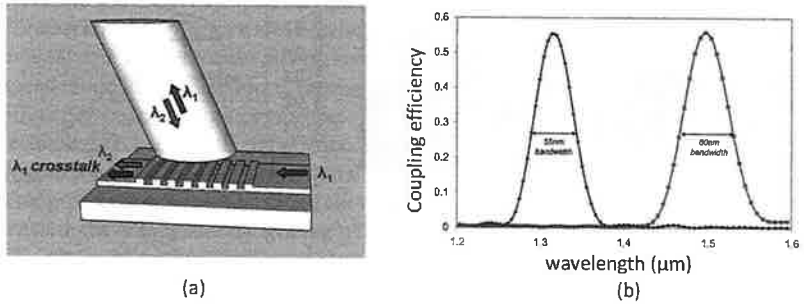

Fig. 3.7 (**a**) Concept of the one-dimensional grating duplexer structure and (**b**) simulated device performance in a silicon overlay grating configuration [10]

(typically −10 dB) is still coupled from the upstream waveguide channel into the downstream waveguide, this can be improved by incorporating a wavelength filter in the downstream wavelength path, in order to combine a high fiber-chip coupling efficiency and low crosstalk behavior. The combination of a one-dimensional grating duplexer and an optical filter to improve the crosstalk performance (and at the same

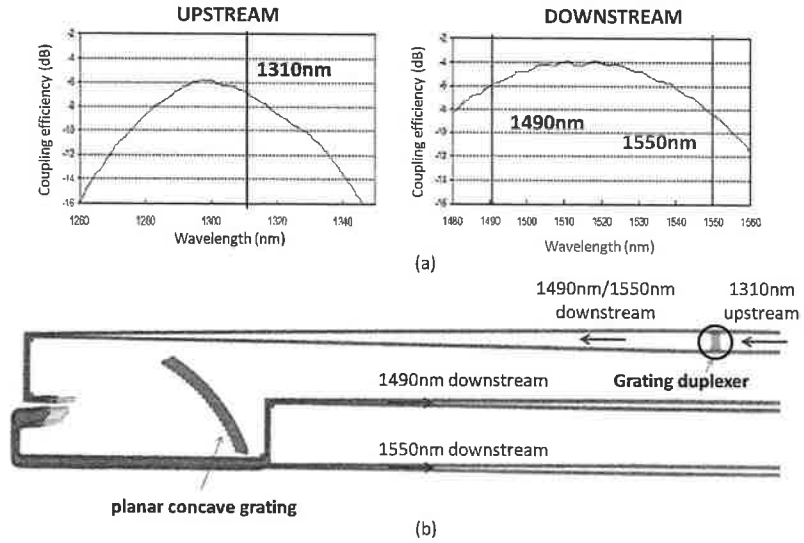

Fig. 3.8 (**a**) Fiber-chip coupling efficiency spectrum for the one-dimensional grating duplexer for the upstream and downstream wavelength channel and (**b**) a microscope image of the fabricated photonic integrated circuit including a one-dimensional grating duplexer and a planar concave grating to split the downstream wavelength channels, while at the same time suppressing the upstream wavelength channel crosstalk to below −30 dB [11]

time split the 1,490 and 1,550 nm wavelength channels) was experimentally realized [11]. In this case, a "standard" grating design was used by directly etching the grating lines into the silicon waveguide layer. The wavelength filter was implemented as a planar concave grating filter, resulting in more than 30 dB suppression of the upstream wavelength channel into the downstream wavelength path and demultiplexing of the 1,490 and 1,550 nm wavelength channels. The fabricated photonic integrated circuit, together with the experimentally obtained fiber-chip coupling spectrum is shown in Fig. 3.8. The device parameters of this device are again listed in Table 3.1.

3.6 Polarization Independent Fiber-Chip Coupling

As described in Sect. 3.3, silicon-on-insulator nanophotonic waveguides experience large modal birefringence, due to the high refractive index contrast of the waveguides and the typical rectangular shape of the photonic wire. This implies that one-dimensional diffraction gratings are inherently very polarization sensitive, since the diffraction angle for transverse electric and transverse magnetic polarized light is substantially different. In most practical applications, however, the polarization of the light in the input optical fiber is unknown and varying over time. While the lateral inverted taper discussed in Sect. 3.2 can be designed to allow for efficient optical coupling for both transverse electric and magnetic polarization, still the photonic components based on these silicon photonic wires behave very differently for both polarizations. This is a well-known issue in high-index contrast waveguide systems. The most popular solution to solve this problem is to use a polarization diversity approach. In this approach, both polarization states are spatially separated in the two arms of the polarization diversity circuit. In the case of a lateral inverted taper structure, first the TE and TM polarized light are spatially separated (e.g., using a directional coupler structure). Then the polarization in one of the arms of the polarization diversity circuit is first rotated to the orthogonal polarization state, thereby allowing the use of identical high index contrast waveguide structures in both arms. However, before combining both arms of the polarization diversity circuit (using an identical polarization combiner structure such as a directional coupler), the polarization needs to be rotated again in one arm [12]. While this approach enables polarization-independent operation of nanophotonic waveguide circuits (which are inherently very polarization dependent), it is clear that this requires several extra integrated optical components (besides the additional requirement of a cleaved and polished facet for optical interfacing).

Because of these drawbacks, we pursued an approach based on diffraction gratings to achieve polarization-independent operation of high-index contrast photonic integrated circuits [13]. The basic idea is to realize a grating structure that is the superposition of two one-dimensional diffraction gratings. Placing these two one-dimensional grating structures orthogonal to each other allows the coupling of both orthogonal polarization states in the optical fiber to the optical waveguide layer. Moreover, the optical modes that are excited by these two orthogonal polarization

states in the orthogonal waveguides have identical polarization (i.e., transverse electric polarization), no longer requiring separate polarization splitter and polarization converter waveguide structures. The superposition of two identical one-dimensional grating structures leads to a square lattice grating for interfacing with the optical fiber. Therefore, a photonic integrated circuit can be made to work in a polarization independent way by incorporating two such square lattice grating structures on a photonic integrated circuit and duplicating the optical functions in both arms of the polarization diversity circuit. The concept of this polarization diversity approach and the operation principle of the square lattice grating structure is schematically shown in Fig. 3.9.

While this is conceptually an easy way to realize polarization-independent operation, two important issues complicate its actual realization. First of all there is the need for identical photonic integrated circuits in both arms of the polarization diversity configuration, which is also the case for the edge-coupling method. Although state-of-the-art deep UV lithography is used, this is far from trivial to achieve. It turns out that deep sub-nanometer dimensional control is required to match for example the resonance frequencies of a silicon ring resonator (a rule of thumb says that one nanometer variation in waveguide dimension results in a one nanometer wavelength shift). One way to tackle this problem is to thermo-optically tune the photonic integrated circuits, to compensate for the non-uniformity. In some applications, however, it is possible to use a single optical component for both arms of the polarization diversity circuit, by passing the light through the device in opposite directions. This mechanism is not limited to the diffraction grating approach and can be used in all polarization diversity approaches. This device concept was demonstrated for the case of polarization independent operation of an SOI arrayed waveguide grating [14] and ring resonator structure [12]. Another difficulty specific to the two-dimensional grating coupler implementation is the fact that the previous reasoning pointing to a square lattice grating structure as a polarization independent

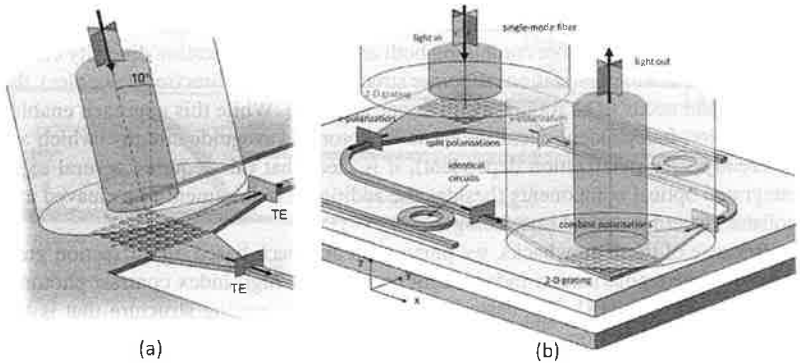

Fig. 3.9 Concept of the two-dimensional square lattice grating as (**a**) a polarization independent interface to the optical fiber and (**b**) the polarization diversity configuration

coupler is, in principle, only valid for a perfectly perpendicular positioned optical fiber. However, in Sect. 3.3 we pointed out that perfectly vertical positioning of the optical fiber results in strong second-order Bragg reflection and associated reduced fiber coupling efficiency. Therefore, a tilt of the optical fiber is still required to interface with a two-dimensional grating structure. To preserve the symmetry of the polarization diversity circuit, this tilt should be along the bisection line of the diffraction grating. This tilt has two implications. First, tilting the optical fiber along the bisection line of the two-dimensional grating implies that the waveguides connected to this grating structure also need to be tilted inwards, as is clear from the projected Bragg condition

$$\boldsymbol{k}_{z,i} = \boldsymbol{k}_{\mathbf{in,proj}} + \boldsymbol{K}_i \tag{3.5}$$

with $i = 1, 2$ and $\boldsymbol{K_1} = \frac{2\pi}{\Lambda}\mathbf{1}_x$, $\boldsymbol{K_2} = \frac{2\pi}{\Lambda}\mathbf{1}_y$. Since

$$\boldsymbol{k}_{\mathbf{in,proj}} = \frac{2\pi n}{\lambda}\sin(\theta_0)\left(\frac{\sqrt{2}}{2}\mathbf{1}_x + \frac{\sqrt{2}}{2}\mathbf{1}_y\right) \tag{3.6}$$

wave vectors $\boldsymbol{k}_{z,1}$ and $\boldsymbol{k}_{z,2}$ are no longer orthogonal to each other, as can be seen in Fig. 3.10.

This can however easily be implemented in the design of the integrated circuit by tilting the access waveguides inwards (i.e., 3.1° tilt for a 10° tilted fiber). A more important issue associated with this tilting is the fact that a perfect polarization independent coupling can nò longer be obtained. This can be understood by looking at the polarization in the optical fiber along the bisection line of the grating and the orthogonal polarization. By tilting the optical fiber, the polarization along the bisection line is tilted out of the plane of the photonic integrated circuit, while the orthogonal polarization stays in this plane, as shown in Fig. 3.11a. This implies

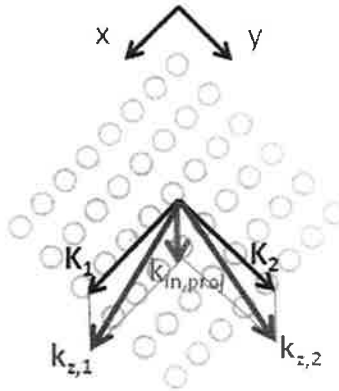

Fig. 3.10 Calculation of the non-orthogonal wave vectors in the silicon waveguide layer due to the finite projected wave vector of the incident light arising from the tilting of the optical fiber

that the coupling spectrum for both polarizations will be different when the fiber is tilted off vertical, resulting in an intrinsic polarization-dependent loss (PDL) of the grating structure. This is confirmed by rigorous three-dimensional FDTD simulations (see Fig. 3.11b), showing the presence of a wavelength-dependent PDL. This wavelength-dependent PDL is also observed in the experiment, as shown in Fig. 3.11c. The parameters of the grating coupler structure are listed in Table 3.1. While this wavelength-dependent PDL arises due to the tilting of the optical fiber, improvement can be expected by optimizing the design of the grating structure. This requires however extensive three-dimensional FDTD simulations and has not been studied in detail so far.

Recently we studied another approach to realize a polarization-independent interface to a silicon photonic integrated circuit, using a one-dimensional grating structure [15]. In this case, the same mechanism as described in Sect. 3.5 is used to interface with both polarizations on the photonic integrated circuit, as shown in Fig. 3.12a. Although this allows one to couple both polarizations to the photonic integrated circuit (and spatially separate them on the chip), the modes in the waveguides still are TE and TM polarized, respectively. This means that a polarization rotator is still required to realize a true polarization diversity scheme. In this case, the grating coupler fulfills the role of fiber-chip coupler and polarization splitter at the same time. In some applications, the need for a polarization converter is not

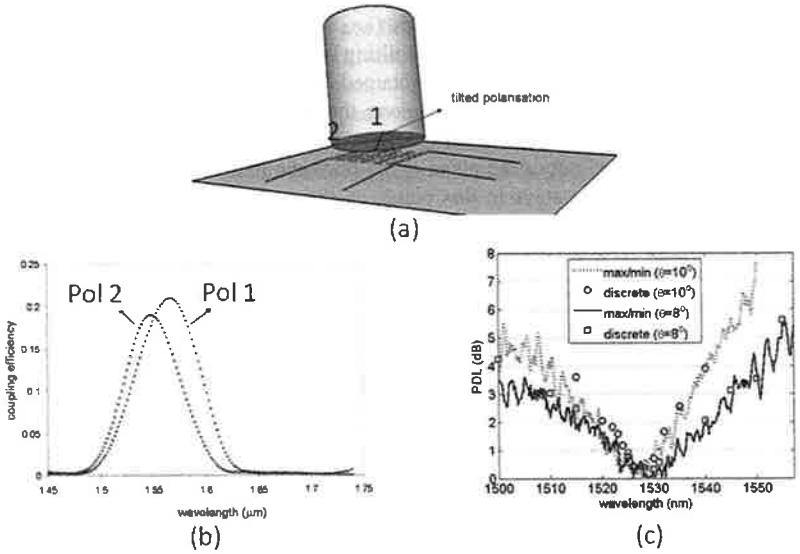

Fig. 3.11 Tilting of the optical fiber and its influence on the polarization-dependent loss: (**a**) schematic, (**b**) rigorous FDTD simulation of the polarization dependence of the coupling efficiency, and (**c**) experimentally obtained polarization dependent loss as a function of the wavelength

even required. This is, for example, the case for a point-to-point transceiver in which the downstream wavelength only needs to be coupled to the chip in a polarization-independent way, where it is immediately detected. By optimization of the grating structure, polarization-independent coupling of the downstream wavelength and single polarization coupling of the upstream wavelength using a one-dimensional grating structure can be realized at the same time. This was recently demonstrated using a standard diffraction grating approach for polarization-independent coupling of a 1,310 nm wavelength signal and single polarization coupling of a 1,610 nm wavelength signal. The operation wavelength of the device is defined both by the grating period and angle of the optical fiber, although the waveguide layer thickness and grating etch depth also play a significant role. Because the device geometry was fixed, the important wavelength combination of 1,310/1,550 nm could not be reached, although a slight modification in waveguide geometry and etch depth allows one to do so. The operation principle of this device was demonstrated using standard diffraction grating structures (a 220-nm-thick silicon waveguide layer and a 70-nm etch depth for the grating). A coupling efficiency of −5.9 dB for the 1,610 nm wavelength channel was obtained, while a −5.2 dB coupling efficiency was obtained for 1,310 nm, which is independent of the polarization of the incident light. The fiber-to-fiber polarization dependent loss measured using this device configuration is lower that 1 dB over a broad wavelength range of 70 nm. The fiber-to-chip coupling efficiency for both wavelength channels and the polarization dependent loss of the

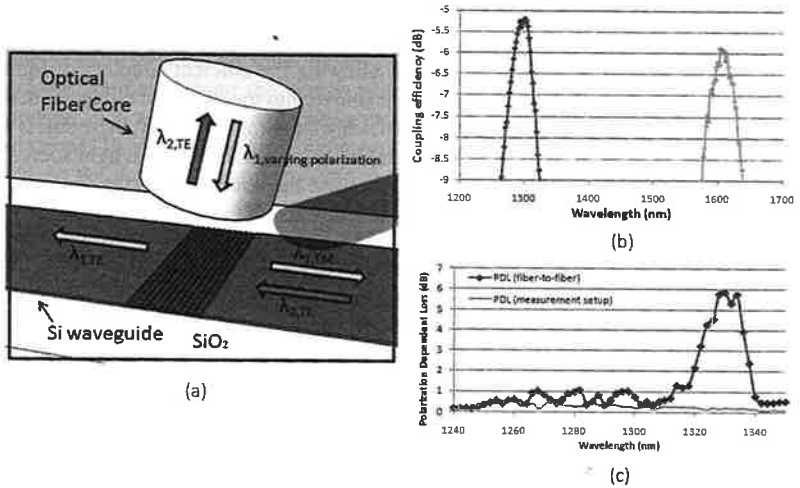

Fig. 3.12 A one-dimensional diffraction grating for polarization independent coupling of a λ_1 wavelength channel and single polarization coupling of an upstream wavelength channel λ_2: (**a**) device principle, (**b**) experimentally obtained fiber coupling spectrum, and (**c**) measured polarization dependent loss for the downstream wavelength channel (**c**)

downstream wavelength channel is shown in Fig. 3.12b and c. The parameters of the grating structure used in the experiment are listed in Table 3.1.

3.7 Integration of Opto-electronic Components

So far we have discussed the use of diffraction gratings as a means to interface with a single-mode optical fiber. The use of grating couplers is however not restricted to this application: interfacing with hybrid integrated III–V opto-electronic components can be envisioned as well. In this case, these opto-electronic components need to be flip-chipped on top of the diffraction gratings. However, one particular aspect of the diffraction gratings needs to be considered with care. In Sect. 3.3 we elaborated on the fact that diffractive grating structures only perform well for oblique diffraction. Otherwise, second-order reflection and reduced coupling efficiency occur. While this is not a problem for a flip-chipped photodetector (or at least can be taken into account in the design), this is a serious issue for vertically emitting laser diodes, like vertical cavity surface emitting lasers (VCSELs). Although there are ways to flip chip components in a tilted fashion, this is not the standard approach. Therefore, to interface a VCSEL with a silicon photonic integrated circuit, a modified grating layout is required.

One approach we have pursued to solve this problem is the modification of the grating structure by adding either a grating at the backside of the coupling grating functioning as a high-reflectivity grating [4], or adding an additional slit at the front side of the grating, acting as an anti-reflection type coating [16]. Both approaches create an asymmetry in the grating design allowing the efficient coupling of light from a flip-chipped vertically emitting light source into the photonic circuit. While this approach allows realizing a high VCSEL-chip coupling efficiency, there still is a parasitic reflection from the grating that couples back into the VCSEL light source. This is an unwanted situation, since it will increase the noise of the laser diode and can even result in polarization switching of the device.

Therefore, an alternative approach was investigated. In this case, an obliquely operating grating coupler structure is used, as discussed in the previous section. To interface with the opto-electronic component, a wedge can be defined on top of the grating structure to refract the light to the surface normal direction, as shown in Fig. 3.13a. This approach has several advantages. First of all, standard diffraction gratings optimized for high-coupling efficiency can be used. Moreover, due to the presence of the wedge, the influence of specular reflection into the laser cavity is significantly reduced, yielding a more stable solution. This approach of integrating a wedge on top of the diffraction grating has recently been demonstrated [17]. In this case, a polymer wedge was defined on top of the grating structures by means of a nanoimprint lithography technique, as shown in Fig. 3.13b. Standard diffraction gratings were used as proof-of-principle components. The performance of these grating coupler structures was assessed by probing the wedge/grating combination using a vertically positioned single-mode fiber and comparing the coupling efficiency thus obtained to the oblique coupling efficiency on a reference grating coupler without the wedge structure. Only a marginal penalty in device performance was observed, showing that wedges with good optical quality can be obtained. To emulate the flip-chip integration process and the influence this process has on the device performance (due to the relatively high temperatures used), the polymer wedge/grating coupler combination was exposed to a 300°C temperature cycle of 10 min. Both the configurations based on SU-8 (MicroChem) wedges and PAK polymer (Toyo Gosei) wedges showed no appreciable degradation in device performance, as is clear from Fig. 3.13c.

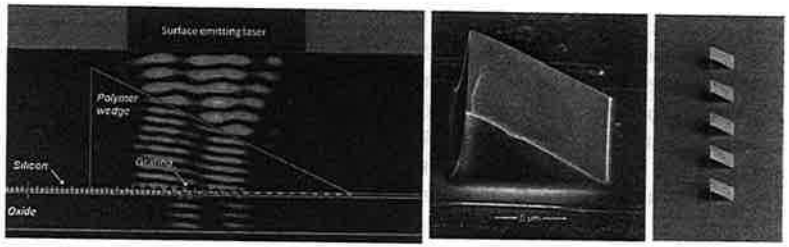

(a) (b)

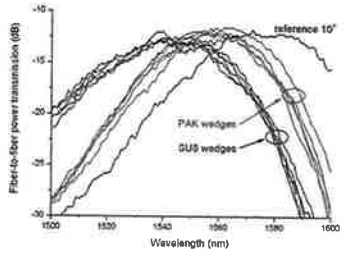

(c)

Fig. 3.13 Integration of a polymer wedge on top of diffractive grating couplers for interfacing with a VCSEL light source: (**a**) FDTD simulation, (**b**) SEM picture of the fabricated structure, and (**c**) measured fiber-to-fiber coupling efficiency after a thermal cycle at 300°C for 10 min [17]

3.8 Small Footprint Fiber-Chip Coupling Structures

While the grating coupler structures presented in the previous sections are very compact (typically 12 by 12 μm in size), a relatively long adiabatic taper is still needed to laterally transform the optical mode size from that of a single-mode fiber (10 μm) to that of a single-mode nanophotonic waveguide (0.5 μm). This taper, on the order of 150 μm in length, determines the footprint of the fiber-chip coupling structure. Since one of the advantages of working on a high refractive index contrast waveguide platform is the density of integration that can be obtained, it would be interesting to

be able to scale down the footprint of the fiber-chip coupling structure. This can be achieved by modifying the layout of the grating structure. Instead of using straight grating lines in a one-dimensional grating structure, a curved grating can be used to couple the light from the fiber to the waveguide plane and at the same time focus the light in that waveguide plane onto the aperture of the optical waveguide. When the waveguide plane is chosen to be the (Y, Z) plane of a right-handed Cartesian coordinate system, with Z along the waveguide axis and the origin chosen to be in the desired focal point, it can be shown that a focusing grating can be obtained by curving the grating lines according to

$$q\lambda_0 = n_{\text{eff}}\sqrt{y^2 + z^2} - zn_t \cos(\theta_c) \tag{3.7}$$

Here, q is an integer number for each grating line, θ_c is the angle between the fiber and the chip surface, n_t is the refractive index of the environment, λ_0 is the vacuum wavelength, and n_{eff} is the effective index felt by the cylindrical wave in the broad waveguide with the grating. The grating lines are ellipses with a common focal point, that coincides with the optical focal point of the coupler. While rigorous design of the focusing gratings would require full three-dimensional simulations, we approximate by extrapolating two-dimensional designs of standard linear gratings for TE-polarization (electric field parallel to the grating lines) and coupling at $\theta_c = 80°$. This way, the use of curved grating structures to reduce the device footprint was demonstrated. We showed that by implementing these curved grating structures an eight-fold reduction in the device footprint is obtained without a penalty in device performance [18].

Besides the demonstration of a one-dimensional curved grating structure, the footprint of a two-dimensional fiber-chip grating coupler can also be scaled down by changing the grating layout. Again the idea is to consider the two-dimensional grating as the superposition of two one-dimensional curved gratings. At the intersection of both one-dimensional curved grating lines, a hole is etched in the silicon

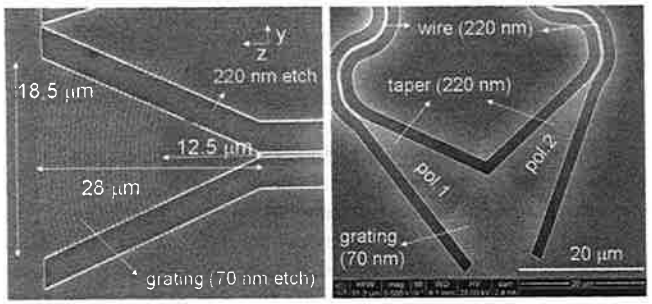

Fig. 3.14 The implementation of compact one-dimensional and two-dimensional curved gratings [18]

waveguide layer, acting as a scatter center. Also in this way, ultra-compact polarization independent coupling to a silicon-on-insulator waveguide circuit was demonstrated without penalty in device performance compared to a standard square lattice two-dimensional grating structure [18]. A one-dimensional and a two-dimensional curved grating structure is shown in Fig. 3.14.

3.9 Optical Probing of Nanophotonic Integrated Circuits

One of the major drivers to use a diffraction grating is the need for interfacing non-singulated chips with an optical fiber. This enables wafer-scale testing of large-scale photonic integrated circuits, comparable to the wafer-scale electronic testing for CMOS circuits. Since both electrical probing and optical probing can be done from the top of the wafer surface, both types of measurements can be combined in a single measurement system, in the case of electronic/photonic integrated circuits. This approach allows using a modified probing station to do a fully automated mapping of the device performance across the wafer. This, however, only allows the characterization of the input-output characteristics of the full photonic integrated circuit, since it is only at the optical input/output ports of the circuit that these grating couplers can be implemented. In the development stage of a photonic integrated circuit, device engineers typically would like to access the individual components in the actual integrated circuit. Therefore, there is the need for a true optical probe, which allows one to do so, without the need for a diffraction grating on the photonic integrated circuit.

The approach we followed for such an optical probe is, instead of defining the diffraction grating on the photonic integrated circuit, to implement a high refractive index contrast grating on the facet of a single-mode optical fiber [19]. By making physical contact between this probe and an input/output waveguide of an individual component of the integrated circuit, a grating coupler is formed allowing the coupling of light to and from the photonic integrated circuit. A prototype fiber probe was realized by defining a uniform metallic periodic structure on the core of a single-mode fiber, by means of an imprint technology. First, the fiber with UV-curable resist on the facet is aligned over a specially prepared mold carrying the 10 by 10 μm gold grating pattern in the mold trenches. The mold was obtained by starting off from an SOI sample containing silicon gratings of 630 nm period and an etch depth of 220 nm. This surface was treated with an antistiction coating. Then, gold was evaporated onto the mold. Finally, the gold on top of the mold grating lines was selectively removed by microcontact printing on another substrate. In this way, the original SOI mold becomes a carrier of the gold grating pattern by leaving the gold only in the grating trenches. After attachment of the fiber to the mold, the cavities are filled and the resist is UV cured. Finally, the mold is released. The metal grating is now attached to the fiber. The fabrication process is schematically outlined in Fig. 3.15a together with an SEM picture of a fabricated device, while Fig. 3.15b

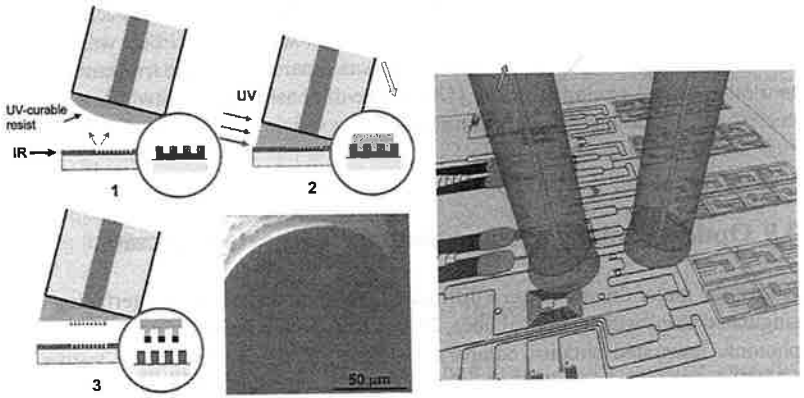

Fig. 3.15 The optical probe: (**a**) probe fabrication and SEM image of a transferred grating onto a fiber facet and (**b**) artist's impression of how the optical probe is used to probe individual integrated optical functions [19]

shows an artist's impression of how this optical probe is used to assess the properties of individual components on a photonic integrated circuit.

Two gold grating fiber probes were fabricated, both consisting of a gold grating of 20 nm thickness. Both probes were brought into contact with a straight 220 nm by 3 μm SOI waveguide. A 15% coupling efficiency and a 1-dB bandwidth of 38 nm was demonstrated in this way for transverse electric polarized light, which is sufficient for testing purposes.

3.10 Conclusions

Diffractive grating structures provide an elegant way of interfacing a high refractive index contrast single-mode fiber and a nanophotonic integrated circuit. Polarization-independent, large optical bandwidth, high-efficiency coupling can be obtained. Even duplexing of two wavelength bands can be realized using the same type of structure. As diffractive grating structures allow accessing a photonic integrated circuit, it paves the way to wafer scale testing of photonic integrated circuits and wafer level packaging of photonic integrated circuits. In this chapter the main focus was on the interfacing of a single mode fiber and a photonic integrated circuit. We showed, however, that it is possible to also interface hybrid integrated opto-electronic components such as flip-chipped photodetectors and VCSELs with the photonic integrated circuit, allowing the realization of complex active/passive photonic integrated circuits. Finally, an optical probe has been presented, creating

the possibility to assess the performance of the individual subcomponents forming the photonic integrated circuit.

Acknowledgments We would like to thank Dr. Dirk Taillaert, Dr. Frederik Van Laere, Dr. Wim Bogaerts, Dr. Jonathan Schrauwen, Dr. Pieter Dumon, Ir. Diedrik Vermeulen, Ir. Shankar Selvaraja, and Prof. Roel Baets for the fruitful discussions.

References

1. W. Bogaerts, D. Taillaert, B. Luyssaert, P. Dumon, J. Van Campenhout, P. Bienstman, D. Van Thourhout, R. Baets, V. Wiaux, S. Beckx, Opt. Express **12**, 1583 (2004)
2. A. Sure, T. Dillon, J. Murakowski, C.C. Lin, D. Pustai, D.W. Prather, Opt. Express **11**, 3555 (2003)
3. S.J. McNab, N. Moll, Yu.A. Vlasov, Opt. Express **11**, 2927 (2003)
4. D. Taillaert, W. Bogaerts, P. Bienstman, T.F. Krauss, P. Van Daele, I. Moerman, S. Verstuyft, K. De Mesel, R. Baets, J. Quantum Electron **38**, 949 (2002)
5. F. Van Laere, G. Roelkens, M. Ayre, J. Schrauwen, D. Taillaert, D. Van Thourhout, T. Krauss, R. Baets, J. Lightwave Technol. **25**, 151 (2007)
6. S. Selvaraja, D. Vermeulen, M. Schaekers, E. Sleeckx, W. Bogaerts, G. Roelkens, P. Dumone, D. Van Thourhout, R. Baets, Highly efficient grating coupler between optical fiber and silicon photonic circuit, p. CTuC6, CLEO, Baltimore, 2009
7. G. Roelkens, D. Van Thourhout, R. Baets, Opt. Express **14**, 11622 (2006)
8. G. Roelkens, D. Vermeulen, D. Van Thourhout, R. Baets, S. Brision, P. Lyan, P. Gautier, J.M. Fedeli, Appl. Phys. Lett. **92**, 131101 (2008)
9. L. Vivien, D. Pascal, S. Lardenois, D. Marris-Morini, E. Cassan, F. Grillot, S. Laval, J.M. Fedeli, L.El Melhaoui, J. Lightwave Technol. **24**, 3810 (2006)
10. G. Roelkens, D. Van Thourhout, R. Baets, Opt. Express **15**, 10091 (2007)
11. D. Vermeulen, G. Roelkens, J. Brouckaert, D. Van Thourhout, R. Baets, R. Duijn, E. Pluk, G. Van den Hoven, Silicon-on-insulator nanophotonic waveguide circuit for Fiber-to-the-Home transceivers, p. Tu3C6, ECOC, Brussels, 2008
12. H. Fukuda, K. Yamada, T. Tsuchizawa, T. Watanabe, H. Shiojima, S. Itabashi, Opt. Express **16**, 4872 (2008)
13. D. Taillaert, H. Chong, P.I. Borel, L.H. Frandsen, R.M. De La Rue, R. Baets, Photon. Technol. Lett. **15**, 1249 (2003)
14. W. Bogaerts, D. Taillaert, P. Dumon, D. Van Thourhout, R. Baets, Opt. Express **15**, 1567 (2007)
15. D. Vermeulen, G. Roelkens, D. Van Thourhout, R. Baets, Silicon-on-insulator polarization independent one-dimensional grating duplexer for fiber-to-chip coupling, submitted for publication in J. Lightwave Technol.
16. G. Roelkens, D. Van Thourhout, R. Baets, Opt. Lett. **32**, 1495 (2007)
17. J. Schrauwen, S. Scheerlinck, D. Van Thourhout, R. Baets, Polymer wedge for coupling VCSELs to a silicon photonic integrated circuit, p. 72180B, PhotonicsWest, San Jose, 2009
18. F. Van Laere, W. Bogaerts, P. Dumon, G. Roelkens, D. Van Thourhout, R. Baets, Group IV photonics **15**, 10091 (2007)
19. S. Scheerlinck, D. Taillaert, D. Van Thourhout, R. Baets, Appl. Phys. Lett. **91**, 031104 (2008)

Appendix

In this appendix the device parameters and measurement conditions for the various types of considered grating coupler structures are listed.

Table 3.1 Parameters of the various types of fiber-to-chip grating coupler structures (DC is the grating duty cycle, n_{sup} is the refractive index of the medium on top of the grating and N is the number of grating periods)

Coupler	Period (nm)	Etch (nm)	DC	Fiber tilt (Degrees)	n_{sup}	N
Standard	630	70	0.5	10	1.0	20
Gold mirror	630	70	0.5	10	1.0	20
DBR bottom mirror	630	70	0.5	10	1.45	20
Silicon overlay	610	250	0.5	10	1.45	20
1D duplexer	520	70	0.5	10	1.45	20
2D coupler	605	70	Diam = 390	10	1.0	Rows = 19
1D pol. div.	535	70	0.5	14	1.45	18

Index

Chapter 4
Development and Application of Er-Doped Silicon-Rich Silicon Nitrides and Er Silicates for On-Chip Light Sources

Jee Soo Chang, Kiseok Suh, Moon-Seung Yang, and Jung H. Shin

Abstract On-chip light sources are a critical part for an integrated Si photonic technology, yet they lag other photonic components in their level of development. In this chapter, Er used as an optical dopant and utilizing its intra-4f transition at 1.54 μm will be introduced as a viable means for on-chip light generation that has the advantage of being compatible with long-distance telecom as well. First, a general introduction to the topic of developing a Si-based/compatible light source will be presented, with emphasis on the need for a novel high-index material for Er-doping that can provide both a higher Er content and refractive index than has been reported so far. Second, Er-doped silicon-rich silicon nitride (SRSN) and Er silicates will be introduced as a promising host material for compact on-chip light sources. Finally, results of fabricating basic photonic components using Er-doped SRSN and Er-silicates will be presented.

4.1 Introduction

4.1.1 Si Photonics and Light Sources

In the developing field of Si photonics, great strides have been made in developing compact active photonic devices such as ultra-fast modulators [1, 2], optical buffers [3], and detectors [4, 5] that seemed impossible just a few years ago. By leveraging the astronomical infrastructure for Si processing, these devices hold the promise of achieving an electronic-photonic convergence on a Si platform that can overcome the "interconnect bottleneck."

J.S. Chang, K. Suh, and M.-S. Yang (✉)
Department of Physics, Korea Advanced Institute of Science and Technology (KAIST), Daejeon, Republic of Korea

J.H. Shin (✉)
Department of Physics; Graduate School of Nanoscience and Technology (WCU), Korea Advanced Institute of Science and Technology (KAIST), Daejeon, Republic of Korea
e-mail: jhs@kaist.ac.kr

D.J. Lockwood, L. Pavesi (Eds.): *Silicon Photonics II.*
Topics in Applied Physics **119**, 95–130 (2011)
DOI 10.1007/978-3-642-10506-7_4

Topics in Applied Physics 119

David J. Lockwood
Editor

Silicon Photonics II
Components and Integration

This book is volume II of a series of books on silicon photonics. It gives a fascinating picture of the state-of-the-art in silicon photonics from a component perspective. It presents a perspective on what can be expected in the near future. It is formed from a selected number of reviews authored by world leaders in the field, and is written from both academic and industrial viewpoints. An in-depth discussion of the route towards fully integrated silicon photonics is presented. This book will be useful not only to physicists, chemists, materials scientists, and engineers but also to graduate students who are interested in the fields of micro- and nanophotonics and optoelectronics.

ISBN 978-3-642-10505-0

springer.com

Lockwood *Ed.*

Silicon Photonics II

David J. Lockwood
Editor

TOPICS IN APPLIED PHYSICS 119

Silicon Photonics II

Components and Integration